Road Materials and Pavement Design

ISSN: 1468-0629 (Print) 2164-7402 (Online) Journal homepage: http://www.tandfonline.com/loi/trmp20

Climate change: potential impacts on frost–thaw conditions and seasonal load restriction timing for low-volume roadways

Jo Sias Daniel, Jennifer M. Jacobs, Heather Miller, Anne Stoner, Jillian Crowley, Masoumeh Khalkhali & Ashley Thomas

To cite this article: Jo Sias Daniel, Jennifer M. Jacobs, Heather Miller, Anne Stoner, Jillian Crowley, Masoumeh Khalkhali & Ashley Thomas (2017): Climate change: potential impacts on frost–thaw conditions and seasonal load restriction timing for low-volume roadways, Road Materials and Pavement Design, DOI: 10.1080/14680629.2017.1302355

To link to this article: http://dx.doi.org/10.1080/14680629.2017.1302355

Published online: 27 Mar 2017.

Road Materials and Pavement Design, 2017
http://dx.doi.org/10.1080/14680629.2017.1302355

Climate change: potential impacts on frost–thaw conditions and seasonal load restriction timing for low-volume roadways

Jo Sias Daniel[a]*, Jennifer M. Jacobs[a], Heather Miller[b], Anne Stoner[c], Jillian Crowley[a], Masoumeh Khalkhali[a] and Ashley Thomas[b]

[a]*Department of Civil and Environmental Engineering, University of New Hampshire, Durham, USA;* [b]*Department of Civil Engineering, University of Massachusetts Dartmouth, N. Dartmouth, USA;* [c]*Climate Science Center, Texas Tech University, Lubbock, USA*

(*Received 25 May 2016; accepted 24 February 2017*)

Low-volume roads constitute a major percentage of roadways around the world. Many of these are located in seasonal frost areas where agencies increase and decrease the allowable weight limits based on seasonal fluctuations in the load carrying capacity of the roadway due to freeze–thaw conditions. As temperatures shift due to changing climate, the timing and duration of winter freeze and spring thaw periods are likely to change, potentially causing significant impacts to local industry and economies. In this study, an ensemble of 19 climate models were used to project future temperature changes and the impact of these changes on the frost depth and timing of seasonal load changes across five instrumented pavement sites in New England. The study shows that shifts of up to 2 weeks are projected at the end of the century and that moderate variability was observed across the study region, indicating that local conditions are important for future assessments depending on the desired level of accuracy. From 1970 to 1999, the average freezing season lasted between 9 and 13 weeks in the study region. By 2000–2029, the frozen period shortens by approximately 10 days over baseline duration (10–20% reduction). By the end of the century under RCP 4.5, frozen periods are typically shorter by 4 weeks or a 30–40% reduction. However, RCP 8.5 results indicate that four out of the five sites would have no frozen period during at least six winters from 2060 to 2089.

Keywords: climate change; low-volume roads; freeze–thaw; seasonal load restrictions; winter weight premiums

Introduction

In the United States, the approximately three million miles of low-volume roads (LVRs) constitute about 70% of the total number of roadways (TranSafety, 1997). LVRs have an annual average daily traffic of 1000 vehicles or less (Faiz, 2012). Approximately half of these LVRs are located in seasonal frost areas, where freeze–thaw processes can result in costly damage to these roadways (Kestler et al., 2011). Freezing conditions make the pavement layers much stiffer and able to support heavier vehicles without causing damage. Transportation agencies take advantage of that period of greater strength by applying winter weight premiums (WWP), increasing the allowable weight trucks can haul during the frozen period (MnDOT, 2014). During spring thaw, the pavement temporarily becomes very weak and highly susceptible to damage. During these times, agencies limit the weight that can travel over a roadway by setting seasonal load restrictions (SLRs). Imposing WWPs and SLRs can have a large impact on the economy of a region

*Corresponding author. Email: jo.daniel@unh.edu

and therefore, there is a strong interest in predicting when these seasonal transitions will occur. Globally, climate-induced warming has been shown to impact the magnitude and timing of seasonal snowpacks (Barnett, Adams, & Lettenmeier, 2005). In the New England region, significant increases in air temperature have been observed with the greatest warming during winter months (Burakowski, Wake, Braswell, & Brown, 2008; Hayhoe et al., 2007). This warming has resulted in an increasing likelihood of rain rather than snow during December and March (Huntington, Hodgkins, Keim, & Dudley, 2004). For natural systems, Campbell et al. (2010) found that projected temperature changes result in a shorter soil frost-covered period. As the climate changes, shifting temperatures will likely cause changes in the timing and duration of the LVRs' winter freeze and spring thaw periods. This study aims to understand how future temperature changes could potentially impact freeze–thaw conditions in LVRs and how variable those changes could be across a region. This study focuses on the Northeastern United States; however, the approach described can be applied to other regions of the nation and world that experience similar issues such as Alaska, Canada, Russia, and Scandinavia.

Background

Climate change

It is now commonly agreed among scientists that the global climate is changing. The Intergovernmental Panel on Climate Change (IPCC) projects increases of the global average temperature between 1.1°C and 4.8°C by the end of the century (Stocker et al., 2013). This affects not only temperature, but a myriad of other variables as well, such as drought, heat waves, sea level, precipitation frequency and amount, and storm and hurricane strength and frequency. Regionally these changes differ, with generally larger increases in temperature projected at higher latitudes. In the northeastern United States, the annual average temperature has already increased by 1.1°C and precipitation by 10% since 1900 (Melillo, Richmond, & Yohe, 2014). Annual average temperatures in the northeastern United States are projected to increase between 1.7°F and 5.6°F towards the end of this century and precipitation is projected to increase, especially in winter and spring, with a higher frequency of heavy rain events (Melillo et al., 2014).

Global climate models (GCMs) that simulate the Earth's atmosphere, oceans, and, depending on the model, land use and the biosphere, make projections of how the future climate might evolve, given a collection of different assumptions (also called scenarios or pathways) concerning social evolution, such as population, energy choices, etc. Climate modelling groups run their models and calculate projections of a large suite of variables for the entire globe (Collins et al., 2013). There are currently about 25 different GCMs.

Although GCMs provide substantial information, the output is typically at a resolution of several hundred miles. This resolution is often too coarse to capture smaller scale variations, due to topography, the coastline, and land use, needed for local or regional assessments. Downscaling techniques can enhance the resolution of the climate projections at local to regional scales. The climate projections used in this work have been downscaled using a statistical downscaling procedure that will be discussed in the Methods section.

Freeze and thaw in LVRs

The freeze–thaw process begins in late fall and concludes in late winter or early spring, depending on the year and geographic location. When air temperatures drop, heat and moisture move upward from subsurface soils in response to the thermal gradient. Frost action begins at the

surface of the pavement and progresses downward, sometimes forming ice lenses that expand and cause frost heaves. When the roadway and subsurface are frozen they can support heavier loads. During this period some agencies allow an increased weight limit for vehicles, called a winter weight premium (WWP), which is a benefit for many hauling industries.

During late winter and early spring, the soil begins to thaw from the surface downward, as well as from the bottom of the frozen layer upward, although the latter generally occurs at a slower rate. Excess moisture is trapped in the upper layers of the roadway by the impermeable underlying frozen soil. The road surface then rests on the weak saturated layer causing the pavement structure to be highly susceptible to damage from heavy loading. Interstate and other primary highways are designed to withstand heavy traffic during spring thaw by using thicker surface layers and non-frost susceptible base soils. Most LVRs are not constructed to those same standards and are thus highly vulnerable. To reduce roadway damage on LVRs, highway agencies apply spring load restrictions (SLR), reducing the allowable loads during this critical time interval.

At the end of the freezing season, the soil thaws completely and the previously trapped excess moisture drains freely via gravity. As a result, the strength and rigidity of the soil recovers, and the roadway is no longer at a high risk for damage. The time it takes for the soil to fully recover could be days or even weeks, depending on soil permeability and local groundwater levels. Ideally, the SLR should remain in place until the strength/stiffness recovery is complete. It should be noted that a pavement structure might go through some temporary thawing near the surface, followed by a re-freezing period prior to the complete thawing in late winter/early spring. Although an LVR may be highly susceptible to damage during those thaw/re-freeze events, existing SLR policies in the United States do not address those windows. It is generally not possible or practical for transportation agencies to apply and remove SLRs during those events, which are currently relatively infrequent and of short duration. With a changing climate, however, it is possible that transportation agencies may need to make some major modifications to SLR policies to address these thaw/re-freeze events.

Clearly, the timing of WWP and SLR application and removal is critical for the longevity of LVRs. The challenge in making those decisions is to protect the infrastructure and minimise roadway maintenance costs, but also to minimise the economic impact on industries responsible for transporting goods on LVRs. For example, in some areas the interruption in hauling goods due to SLRs may last as long as 25% of the year, strongly impacting timber industries for example (Kestler et al., 2011).

Historically, transportation agencies have imposed SLRs based on set dates and/or visual inspection procedures. Using fixed dates creates an issue since subsurface freezing and thawing patterns vary from year to year: appropriate dates and durations for 1 year may not be appropriate for other years. In the inspection/observational approach, field personnel observe changes in the roadways in the early spring, such as rutting, cracking, water seepage, and/or other indicators of pavement distress. By the time pavement issues are observed, the agency has essentially committed to allowing some level of damage, as legislation normally requires 3–5 days' notice prior to applying SLRs. Additionally, this method tends to be highly subjective.

Highway agencies are now becoming more interested in establishing WWP and SLR applications and durations according to science-based decisions rather than using pre-set calendar dates or individual judgement. Some agencies are using quantitative approaches to monitor spring thaw processes, such as measuring pavement deflections with a falling weight deflectometer (FWD), and back calculating layer moduli or other indices. Other agencies have installed sensors beneath roadways to monitor subsurface temperature and/or moisture profiles during the winter freeze and spring thaw periods. Recent research has led to the development of protocols and models that are driven by atmospheric weather forecasts to provide advance warning of estimated dates when

WWPs and SLRs should be placed and lifted. Miller et al. (2015) conducted a comprehensive review of these protocols/models.

Regardless of the approach used by decision-makers for WWP and SLR timing, it is clear that as our climate changes, appropriate dates for placing and removing WWPs and SLRs will evolve. The objective of this study was to use projected air temperatures from an ensemble of climate models to forecast how climate change might impact freeze and thaw processes beneath roadways and how these impacts may vary across a region. The results of this study are intended to help transportation agencies plan for future adjustments in roadway management as the climate changes.

Methods

Projections for the optimum times to apply WWPs and SLRs were calculated for the five test sites shown in Figure 1, all located in northern New England. This study used a widely accepted protocol developed by the Minnesota Department of Transportation (MnDOT) for applying WWPs based on a cumulative freezing index (CFI) threshold, and SLRs based on a cumulative thawing index (CTI) threshold (MnDOT, 2014). The CFI and CTI are calculated based on observed and forecasted daily minimum and maximum air temperatures. Although other different but equally valid approaches to SLR management are utilised in Alaska, Canada, and the Scandinavian countries, the MnDOT guidelines were selected for this study because previous research at test sites in northern New England showed a good correlation between the MnDOT CTI threshold and thaw weakening, as indicated by FWD testing (Miller, Cabral, Kestler, Berg, & Eaton, 2013). Additionally, several transportation officials in northern New England are moving towards use of the MnDOT protocol in making their posting decisions. For projected air temperature input to compute CFI and CTI, this study used gridded statistically downscaled Coupled Model Intercomparison Project Phase 5 (CMIP5) multi-model ensemble output from the Bureau of Reclamation (Brekke, Thrasher, Maurer, & Pruitt, 2013) that provides projected daily minimum and maximum air temperatures from 2000 to 2099 under two greenhouse gas emission scenarios (RCP 4.5 and RCP 8.5) along with gridded observed climate (Maurer, Wood, Adam, Lettenmaier, & Nijssen, 2002) and CMIP5 climate model output for 1950–1999. The downscaled daily temperature values were also used as input to a modified version of the Army Corps Model 158 (Miller et al., 2015) to predict daily frost and thaw profiles beneath the roadway test sites on a seasonal basis until 2099.

The following subsections describe the climate models utilised to obtain projected air temperatures, the equations involved in computing the CFI, the CTI, and predicted frost and thaw depths, and the details of the study test sites.

Climate models

Downscaled climate model output was obtained from the Bureau of Reclamation for 19 GCMs from the CMIP5 archive. The 19 models, listed in Table 1, have been statistically downscaled to 1/8th degree resolution over the continental United States using the Bias-Correction and Spatial Disaggregation technique (Wood, Maurer, Kumar, & Lettenmaier, 2002). The model output used here consists of daily minimum and maximum temperatures for the grid cells containing each of the test site locations for the period 2000–2099. Two emission scenarios were chosen, RCP 4.5 and RCP 8.5, to achieve two realistic overall trends encompassing both lower and higher emission scenarios that also consider the variability of future greenhouse gas emissions. All GCMs that had output for both emission scenarios were chosen. A baseline time period of 1950–1999 was used to validate the model calculations against observations.

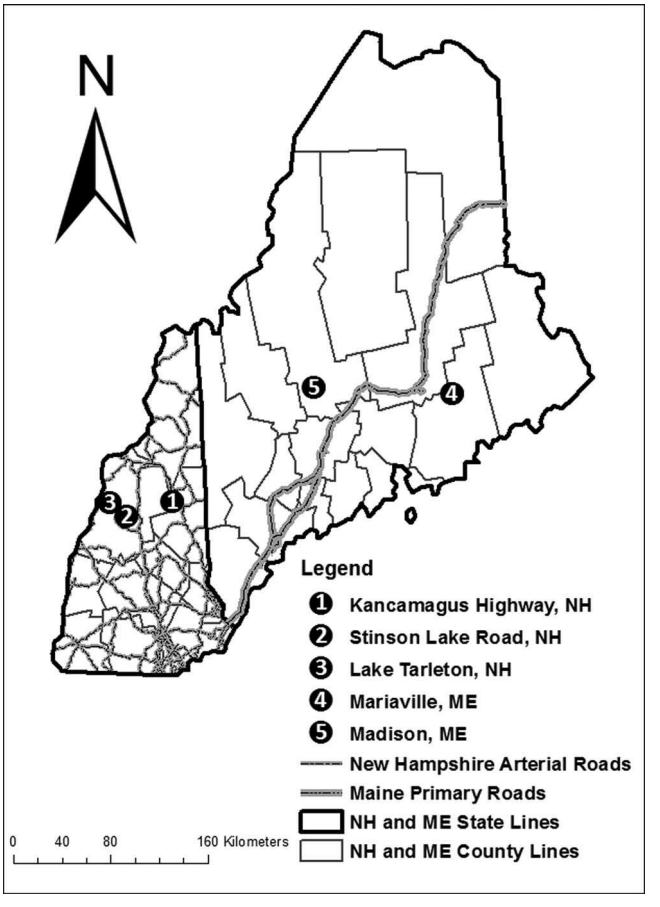

Figure 1. Project test site locations in New Hampshire and Maine, USA.

Freezing and thawing indices

The freezing and thawing indices for this project generally follow the MnDOT (2014) guidelines, with slight modification as outlined below. The freezing index computations begin once the daily average air temperature drops below freezing, as follows:

$$\mathrm{FI}_i = \left(T_{\mathrm{ref}} - \frac{T_{\max} + T_{\min}}{2}\right), \tag{1}$$

$$\mathrm{CFI}_n = \sum_{i=1}^{n} \mathrm{FI}_i, \tag{2}$$

where FI_i is the daily freezing index for day i (°C days); T_{ref} is the MnDOT reference temperature (as described below); $T_{\max}$ and $T_{\min}$ are the daily maximum and minimum air temperatures, respectively, for day i (°C); CFI_n is the cumulative freezing index for day n (°C days). (Note that the CFI is reset to zero on any day when $\mathrm{CFI}_n < 0$.)

The use of a reference temperature was recommended by the MnDOT to compensate for the temperature differential between the air temperature and the asphalt surface temperature. In Minnesota, it was found that the air temperature required for pavement thawing to begin actually decreases during the early spring, probably due to the increase in the elevation angle of the sun

Table 1. Climate models from the CMIP5 multi-model ensemble included in the study.

Modelling centre (or group)	Institute ID	Model name
Commonwealth Scientific and Industrial Research Organization (CSIRO) and Bureau of Meteorology (BOM), Australia	CSIRO-BOM	ACCESS1.0
Beijing Climate Center, China Meteorological Administration	BCC	BCC-CSM1.1
Canadian Centre for Climate Modelling and Analysis	CCCMA	CanESM2
National Center for Atmospheric Research	NCAR	CCSM4
Community Earth System Model Contributors	NSF-DOE-NCAR	CESM1(BGC)
Centre National de Recherches Météorologiques/Centre Européen de Recherche et Formation Avancée en Calcul Scientifique	CNRM-CERFACS	CNRM-CM5
Commonwealth Scientific and Industrial Research Organization in collaboration with Queensland Climate Change Centre of Excellence	CSIRO-QCCCE	CSIRO-Mk3.6.0
NOAA Geophysical Fluid Dynamics Laboratory	NOAA GFDL	GFDL-ESM2G GFDL-ESM2M
Institute for Numerical Mathematics	INM	INM-CM4
Institut Pierre-Simon Laplace	IPSL	IPSL-CM5A-LR IPSL-CM5A-MR
Japan Agency for Marine-Earth Science and Technology, Atmosphere and Ocean Research Institute (The University of Tokyo), and National Institute for Environmental Studies	MIROC	MIROC-ESM MIROC-ESM-CHEM
Atmosphere and Ocean Research Institute (The University of Tokyo), National Institute for Environmental Studies, and Japan Agency for Marine-Earth Science and Technology	MIROC	MIROC5
Max-Planck-Institut für Meteorologie (Max Planck Institute for Meteorology)	MPI-M	MPI-ESM-MR MPI-ESM-LR
Meteorological Research Institute	MRI	MRI-CGCM3
Norwegian Climate Centre	NCC	NorESM1-M

(Van Deusen, Schrader, Bullock, & Worel, 1998). Therefore, MnDOT implemented a variable reference temperature to account for increased solar gain. MnDOT recommended using a reference temperature of 0°C until January 31. The solar gain is then accounted for by using a reference temperature of -1.5°C during the first 7 days of February, and thereafter, a further depression of -0.5°C every week until the end of May (MnDOT, 2014).

Thawing index computations typically begin during the late winter/early spring once the daily average temperatures begin warming above freezing. The CTI was computed as follows:

$$\mathrm{CTI}_n = \sum_{i=1}^{n} (\mathrm{DTI} - (0.5 * \mathrm{DFI})). \tag{3}$$

The use of Equation (3) is subject to the following conditions:

(a) When: $(((T_{\max} + T_{\min})/2) - T_{\mathrm{ref}}) < 0^{\circ}\mathrm{C}$
Then: $\mathrm{DTI} = 0^{\circ}\mathrm{C}$ day, and $\mathrm{DFI} = (0^{\circ}\mathrm{C} - (T_{\max} + T_{\min})/2)$

(b) When $(((T_{max} + T_{min})/2) - T_{ref}) \geq 0°C$
Then: DTI $= (((T_{max} + T_{min})/2) - T_{ref})$ and DTI $= 0°C$ day
(c) CTI is reset to zero on any day when $CTI_n < 0$

where CTI_n is the cumulative thawing index for day n (°C days); DFI and DTI are the daily freezing and thawing indices, respectively, for day i (°C days); T_{max} and T_{min} are the daily maximum and minimum temperatures, respectively, for day i (°C days); T_{ref} is the MnDOT reference temperature (°C).

In the CTI equation, the freezing index is multiplied by a re-freeze factor of 0.5 to account for the partial phase change of water from a liquid to semi-solid during temporary re-freeze events.

WWP and SLR timing thresholds

For WWP application, MnDOT (2014) recommends allowing increased axle loads when the 3-day weather forecast indicates that the CFI will exceed 156°C-days, and "extended forecasts predict continued freezing temperatures." The end date of the WWP period is determined when forecasted air temperatures predict daily thawing, as indicated by the CTI, and the impending placement of SLR. MnDOT recommends that the SLR should be applied when the 3-day weather forecast indicates that the CTI will exceed 14°C-days, and "longer-range forecasts predict continued warmth." The authors interpret this to mean that if forecasts show the CTI temporarily rising above the 14°C-day threshold, but then colder weather pushes the CTI back down below that threshold, the SLR would not yet be applied.

Frost and thaw depth prediction: Modified Model 158

The United States Army Corps of Engineers New England Division (Division, 1949) examined several frost prediction models. One of the equations in that report was Model 158, which was similar to the Modified Berggren equation (Andersland & Ladanyi, 2004), using air temperature indices as well as pavement material properties to integrate heat flow into the calculation of maximum seasonal frost depth. That model was modified by Orr and Irwin (2006), and later by Miller et al. (2015), to enable prediction of both frost and thaw depths on a daily basis. For this study, frost and thaw depths were predicted using the equations shown below.

$$(X_f)_n = -\frac{d}{2} + \left[\left(\frac{d}{2}\right)^2 + \frac{86,\ 400 M_f\, k (I_{sf})_n}{L + c(v_0 + (I_{sf})_n/2t)}\right]^{1/2}, \tag{4}$$

$$(X_t)_n = -\frac{d}{2} + \left[\left(\frac{d}{2}\right)^2 + \frac{86,\ 400 M_f\, k (I_{st})_n}{L + c(v_0 + (I_{st})_n/2t)}\right]^{1/2}, \tag{5}$$

where $(X_f)_n$ is the depth of frost on day n (m); $(X_t)_n$ is the depth of thaw on day n (m); d is the thickness of the surface asphalt layer (m); $(I_{sf})_n$ is the cumulative surface freezing temperature index for day n (°C-days); $(I_{st})_n$ is the cumulative surface thawing temperature index for day n (°C-days); M_f is the multiplier for frost depth computation; M_t is the multiplier for thaw depth computation; k is the thermal conductivity (W/m°C)); L is the volumetric latent heat of fusion (MJ/m^3); c is the volumetric heat capacity (MJ/m^3-°C); v_o is the difference between the mean annual surface temperature and the freezing temperature (°C); t is the annual length of time below freezing (days); 86,400 seconds in a day for dimensional consistency (s/day).

The differences between air freezing and thawing indices, and pavement surface freezing and thawing indices, are accounted for by using *n*-factors:

$$(I_{sf})_n = n_f\,(\mathrm{CFI}_n), \tag{6}$$

$$(I_{st})_n = n_f\,(\mathrm{CTI}_n), \tag{7}$$

The CFI and CTI were computed as previously described in Equations (2) and (3), with the additional stipulation that if there is no frost to be thawed (i.e. frost depth for previous day is zero), then the CTI is set to zero. Values used for *n*-factors ($n_f = 0.9$ and $n_t = 2.0$) were chosen empirically (Andersland & Ladanyi, 2004).

The Modified Model 158 equations require details regarding the pavement structure, specifically the material layer thicknesses and thermal properties. Recommended values for the thermal properties vary by reference. They are a function of multiple parameters, such as soil type, density, temperature, and moisture content. The current code for the Modified Model 158, however, is not set up to incorporate changes in thermal properties as a function of those parameters (which change during the freeze–thaw process), so constant values for *k*, *c,* and *L* must be selected for each material layer in that model. The thermal properties assumed for analysis during this study were estimated based upon correlations developed by Kersten (1949), as outlined in Bianchini and Gonzalez (2012). For the multi-layered structures in this study, the thermal property values (*k*, *c*, and *L*) utilised in the Modified Model 158 were calculated using a weighted average of the values for the layers above the freeze line of the previous day. For example, the *k*-value used for calculating frost depth $(X_f)_n$ on day "*n*" is calculated as:

$$k_n = \frac{k_1 d_1 + k_2 d_2 + k_3 d_3}{(x_f)_{n-1}}, \tag{8}$$

where d_i and k_i are the thickness and thermal conductivity, respectively, of each material layer located above the depth of frost penetration on day $n - 1$, $(X_f)_{n-1}$. If a material layer is located partially above the frost line, and partially below it, then d_i is taken as the thickness of that part of the layer located above the frost line.

The length of the freezing season, *t*, was set to 140 days and the mean annual air temperature, $v_{o,}$ was set to 12°C, following the recommendations from the ModBerg model, a tool to calculate frost depth penetration (Cortez, Kestler, & Berg, 2000). ModBerg utilises a database of temperature data from a 20-year ± collection period at numerous locations, several of which are near the New England test sites. The mean annual surface temperature (for computing v_o) was estimated from the mean annual air temperature using an *n*-factor approach as outlined in Berg, Kestler, Eaton, and Benda (2006).

The multipliers M_f and M_t were added into the Modified Model 158 equations to allow for site-specific calibration of the model in cases where measured frost and thaw depths are available. Site-specific calibration can be conducted by running the Modified Model 158 in a trial-and-error mode, and adjusting M_f and M_t values until a good fit is obtained between measured frost and thaw depths and those predicted from the model. Details of site-specific calibration for two of the five sites included in this study are presented in the following section.

Test sites and pavement conditions

The five test sites, shown in Figure 1, were selected for two reasons. First, the sites are instrumented with temperature sensors to measure frost and thaw depths beneath the roadway. Second, good agreement was found between those measured depths and the frost and thaw depths predicted using the Modified Model 158 during several years of data collection (Miller et al., 2015).

There was also generally good agreement between the onset of freezing and thawing, and the CFI and CTI criteria set by MnDOT (2014) for applying WWPs and SLRs, respectively (Miller et al., 2013).

During the *in-situ* temperature sensors' installation, standard penetration test N-values were recorded and soil samples were collected to classify base, sub-base, and subgrade soils. The soil samples were subjected to grain size analysis (sieve and, in some cases, hydrometer tests), moisture content, and liquid and plastic limit tests (if appropriate). The pavement structure at each site (material layer thickness and description) is shown in Table 2. Material thermal properties, used to predict frost and thaw depths in the Modified Model 158, are also included in this table. As noted previously, the thermal properties were estimated based upon correlations developed by Kersten (1949), as outlined in Bianchini and Gonzalez (2012).

Frost and thaw depths were projected for three of the five test sites (Madison (MAD), Mariaville (MAR), and Stinson Lake (STI)) using the site-specific pavement cross-section, as well as the two generic pavement structures that are typical of low-volume roadways in northern New England. The assumed properties of those two generic pavement cross-sections are shown in the last two rows in Table 2. For those three test sites, site-specific calibrations were not required to obtain good agreement between measured and predicted frost and thaw depths during several years of data collection (i.e. M_f and M_t were both set to a value of 1.0 in the Modified Model 158).

For the remaining two test sites (Lake Tarleton (LAK) and Kancamagus (KAN)), it was necessary to modify M_f and/or M_t to obtain a good match between measured and predicted frost and thaw depths. At those two sites, M_f and M_t values of 1.0 resulted in predicted frost depths that were less than measured depths, and predicted thawing occurring earlier than indicated by thermistors. Site-specific calibration was therefore conducted by running the Modified Model 158 in a trial-and-error mode, and adjusting M_f and M_t values until a good match was achieved between measured frost and thaw depths and those predicted from the model. Calibration resulted in M_f values of 1.5 and 3.5, and M_t values of 1.0 and 0.8 for the LAK and KAN Highway sites, respectively. The need for site-specific calibration may result from characteristics of the pavement structure itself, from characteristics of the site (shallow bedrock, groundwater conditions, shaded versus sunny exposure, etc.), or from both. Therefore, the generic pavement structure was not used to project future frost and thaw depths at the two sites requiring site-specific calibration.

Results

Cumulative freezing and thawing indices

At each of the five analysis sites, the dates at which the CFI and CTI thresholds are projected to be exceeded were determined for each of the 19 climate models under the low (RCP 4.5) and high (RCP 8.5) emission scenarios from 1950 to 2099. Figures 2 and 3 show the dates that the CFI and CTI thresholds will be exceeded for the MAD, ME site. The observed dates (solid line) were calculated via Equations (2) and (3) using measured daily air temperatures from a long-term Global Historical Climatology Network (GHCN) site at MAD, ME (GHCN ID: USC00174927). The projected values were calculated via Equations (2) and (3) using the downscaled climate projections for each climate model in the ensemble. The dashed and dotted lines are the 21-year moving average (year $\pm$ 10 years) of 19 climate models under the high and low emission scenarios, respectively. The shaded areas represent the 95% confidence interval for the 19 climate models. The projected dates for the high-emission scenario end just after 2050 because after that date 5 or more of the 19 models indicated that the CFI threshold would not be exceeded (i.e. pavement may not fully freeze).

Table 2. Pavement structure and material properties at project sites.

Site	Layer	Thickness (cm)	k (W/m°C)	c [MJ/(m^3 °C)]	L [MJ/(m^3)]
Madison, ME (MAD)	HMA	15.2	1.4	1.9	0
	M. Dense, well-graded sand, some gravel	45.7	1.7	1.7	43
	Silty clay subgrade	inf	2.2	2.6	142
Mariaville, ME (MAR)	HMA	15.2	1.4	1.9	0
	Loose, well-graded sand, some gravel	30.5	1.0	1.4	27
	Loose silty sand, little gravel	30.5	1.9	1.8	66
	Dense silty sand, some gravel	61.0	2.4	1.9	52
	Dense poorly graded sand, little gravel	inf	2.3	1.8	56
Lake Tarleton, NH (LAK)	HMA	22.9	1.4	1.9	0
	M. Dense well-graded sand	68.6	2.1	1.7	56
	Loose poorly graded sand	68.6	3.1	2.4	143
	M. Dense silty sand subgrade	inf	3.8	2.2	72
Kancamagus, NH (KAN)	HMA	12.2	1.4	1.9	0
	Crushed gravel	25.4	2.4	1.8	35
	Gravel/sand	66.0	2.0	1.7	34
	Dense well-graded sand, Some gravel (outwash)	inf	2.5	2.0	65
Stinson Lake Rd, NH (STI)	HMA	24.4	1.4	1.9	0
	Loose C-F sand, some gravel (fill)	67.1	2.5	2.1	96
	M. Dense fine sand, little med. sand and silt (outwash)	91.4	2.5	2.4	117
	M. Dense fine sand, some silt, little M-C sand (Till)	inf	3.5	2.2	72
Generic 1: Silty clay subgrade (GEN1)	HMA	10.2	1.4	1.9	0
	Granular base	20.3	2.0	1.7	39
	Silty clay subgrade	inf	2.1	2.3	119
Generic 2: Granular (glacial till) Subgrade (GEN2)	HMA	10.2	1.4	1.9	0
	Granular base	20.3	2.0	1.7	39
	Granular (glacial till) subgrade	inf	2.7	1.9	36

Note: HMA, hot mixed asphalt.

Figures 2 and 3 show, under projected future climate for MAD, ME, the general trend is that the CFI exceedance date will occur later and the CTI exceedance date will occur earlier. As a result, the length of the freezing season will become shorter or disappear altogether. The projections

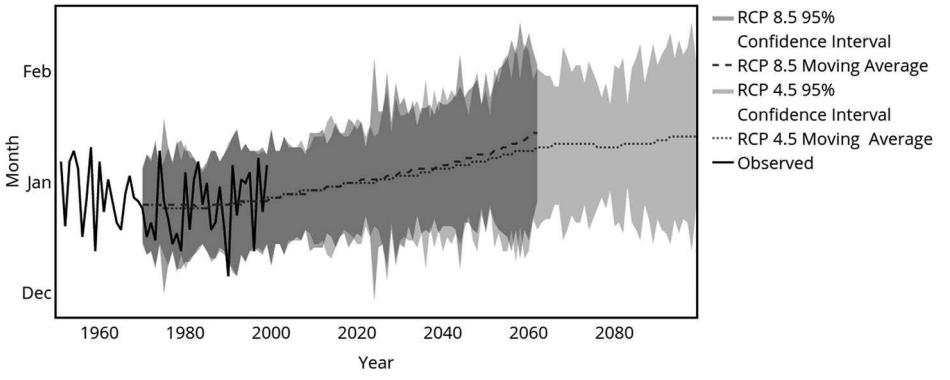

Figure 2. Observed and projected dates that the CFI threshold is exceeded for MAD, ME based on RCP 4.5 and RCP 8.5 using a 21-year moving average. Shaded areas reflect the 95% confidence intervals of the climate models. After 2060, the winter weight threshold was not exceeded in five or more of the climate models.

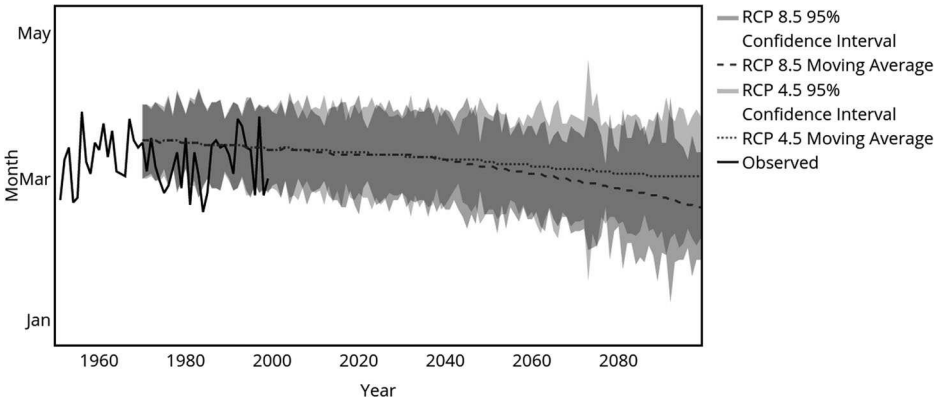

Figure 3. Observed and projected dates the CTI threshold is exceeded for MAD, ME based on RCP 4.5 and RCP 8.5 using a 21-year moving average. Shaded areas reflect the 95% confidence intervals of the climate models.

under the low and high-emission scenarios are similar through mid-century. After approximately 2040, the average trends for the two scenarios differ with the high-emission scenario projecting a larger and more rapid change than the low-emission scenario. The uncertainty in the climate projections, as represented by the 95% confidence interval shaded areas, increases for both the low- and high-emission scenarios toward the end of the century, due to the spread increasing among model projections towards the end of the century. The results for the four other sites (not shown) are similar to the results at the MAD, ME, site.

The temporal evolution for projected CFI and CTI dates for the five sites are compared in Figures 4 and 5, respectively. Tables 3 and 4 summarise the average dates that the CFI and CTI thresholds are exceeded during the historic period (1970–1999), the early (2000–2029), mid (2030–2059), and end of century (2060–2089) periods by emission scenario. Historically, CFI thresholds were exceeded between mid-December to early January across the study region (approximately 150 km × 300 km). This 2-week range reflects differences in local climate and conditions across the study sites. CFI thresholds are projected to be exceeded approximately 1 week later in the early century and 2 weeks later by mid-century, regardless of the emission

scenario. The end-of-century changes depend strongly on the emission scenario. The lower emission scenario results in thresholds that are slightly later than 2 weeks as compared to the historic period. In the higher emission scenario, most models project that the CFI thresholds will not be exceeded at all by the end of the century. CTI trends are similar, but have a more moderated pattern with thaws occurring on the order of 3–4 days earlier and 7–10 days earlier for the early and mid-century periods, respectively.

While represented as a single line, these future values are the average of an ensemble of model runs. For the early century, there is limited variation among models. The models consistently indicate later CFI threshold exceedances with a standard deviation on the order of 3–4 days among the 19 models. By the end of the century, the standard deviation increases to approximately 5 days. This indicates somewhat greater variability among the models, but this variability is much smaller than the overall shift of nearly 20 days. A similar trend of earlier CTI dates is also evident. However, there is more variability more among models for the future CTI dates as compared to the CFI dates.

There is a range of projected CFI and CTI threshold exceedance dates across study sites, the largest being 2 weeks between STI and MAR. Differences between locations that are geographically close are nearly a week in some cases and only a day or two in other cases. The sites that freeze first generally also thaw later: the longest frozen period occurs at the STI Road site, according to this analysis. Of the five sites evaluated, the MAR site has the latest exceedance of the CFI threshold and the earliest exceedance of the CTI threshold, indicating this location will have the shortest period of frozen pavement (Table 5). For baseline years, the average freezing season lasted between 9 and 13 weeks depending on the site. For all sites, the length of the frozen period shortens by approximately 10 days over each 30-year window under the low-emission scenario, with slightly larger decreases under the high-emission scenario. By 2000–2029, the frozen period shortens by approximately 10 days over baseline duration or equivalent to a 10–20% reduction. The mid-century frozen periods are typically shorter by 3 weeks or a 20–35% reduction with the approximately a 5-day difference between low- and high-emission scenarios at each site. By the end of the century under RCP 4.5, frozen periods are typically shorter by 4 weeks or a 30–40% reduction. However, RCP 8.5 results indicate that four out of the five sites had no frozen period during at least six winters from 2060 to 2089.

The two emission scenarios are very similar until approximately 2040, when the high-emission scenario becomes distinct from the lower emission scenario and follows a rapidly changing path. The rate of change with the low-emission scenario slows and appears to approach a peak value slightly before the end of the century. The high-emission scenario line for all sites ends before the competition of the analysis period because five or more models indicate that the CFI is never exceeded at that site. This is also the case for the MAR site under the low-emission scenario. Figures 6 and 7 show the average number of times the CFI is not exceeded for all five sites under low- and high-emission scenarios, respectively. Some sites, like MAR, have a large number of models projecting that the CFI will not be exceeded, even under the low-emission scenario. This indicates that there is a greater probability that the pavements at these sites will not freeze to depths sufficient to warrant WWP application more frequently in the future. For all sites, the number of times the CFI is not exceeded increases with later time periods with the increase being greater under the high-emission scenario.

Frost depths

Projected frost depth for each site was calculated using the Modified Model 158 and the climate model output from the 19 different models under both low (RCP 4.5) and high (RCP 8.5) emission scenarios. Pavement structures and thermal properties described above were used in

Table 3. Average dates that the CFI thresholds are exceeded during the historic period (1970–1999), the early (2000–2029), mid (2030–2059), and end-of-century (2060–2089) periods by emission scenario and site. The standard deviation is determined from 19 model CFI dates. NA values indicate that less than 80% of the models exceeded the CFI threshold.

	Stinson Lake (STI)				Madison (MAD)				Mariaville (MAR)				Kancamagus (KAN)				Lake Tarleton (LAK)			
Periods	RCP 4.5	SD (days)	RCP 8.5	SD (days)	RCP 4.5	SD (days)	RCP 8.5	SD (days)	RCP 4.5	SD (days)	RCP 8.5	SD (days)	RCP 4.5	SD (days)	RCP 8.5	SD (days)	RCP 4.5	SD (days)	RCP 8.5	SD (days)
Baseline (1970–1999)	18-Dec	1.4	18-Dec	1.4	25-Dec	1.4	25-Dec	1.4	2-Jan	1.7	2-Jan	1.7	22-Dec	1.6	22-Dec	1.6	24-Dec	1.9	24-Dec	1.9
Early century (2000–2029)	23-Dec	2.5	25-Dec	2.6	31-Dec	2.5	1-Jan	2.2	10-Jan	2.7	10-Jan	2.5	28-Dec	2.4	28-Dec	2.1	31-Dec	2.7	30-Dec	2.6
Mid-century (2030–2059)	31-Dec	3.6	1-Jan	5.0	7-Jan	3.9	9-Jan	4.7	NA	NA	NA	NA	5-Jan	3.6	6-Jan	5.1	7-Jan	4.1	9-Jan	3.9
End century (2060–2089)	3-Jan	5.1	12-Jan	4.7	12-Jan	5.1	NA	NA	NA	NA	NA	NA	9-Jan	5.1	NA	NA	11-Jan	5.8	NA	NA

Table 4. Average dates that the CTI thresholds are exceeded during the historic period (1970–1999), the early (2000–2029), mid (2030–2059), and end-of-century (2060–2089) periods by emission scenario and site. The standard deviation is determined from 19 model CTI dates.

	Stinson Lake (STI)				Madison (MAD)				Mariaville (MAR)				Kancamagus (KAN)				Lake Tarleton (LAK)			
Periods	RCP 4.5	SD (days)	RCP 8.5	SD (days)	RCP 4.5	SD (days)	RCP 8.5	SD (days)	RCP 4.5	SD (days)	RCP 8.5	SD (days)	RCP 4.5	SD (days)	RCP 8.5	SD (days)	RCP 4.5	SD (days)	RCP 8.5	SD (days)
Baseline (1970–1999)	20-Mar	2.1	20-Mar	2.1	14-Mar	1.3	14-Mar	1.3	8-Mar	2.0	8-Mar	2.0	17-Mar	2.3	17-Mar	2.3	14-Mar	1.8	14-Mar	1.8
Early century (2000–2029)	16-Mar	2.8	18-Mar	3.5	12-Mar	3.2	12-Mar	3.1	3-Mar	2.9	4-Mar	3.7	13-Mar	3.0	15-Mar	3.4	9-Mar	4.1	11-Mar	4.1
Mid-century (2030–2059)	13-Mar	4.3	11-Mar	5.1	9-Mar	3.9	6-Mar	4.5	1-Mar	4.4	25-Feb	4.6	12-Mar	4.2	7-Mar	4.9	5-Mar	4.5	4-Mar	4.5
End century (2060–2089)	9-Mar	6.3	26-Feb	5.7	4-Mar	5.6	22-Feb	5.4	21-Feb	5.9	12-Feb	8.8	7-Mar	5.9	24-Feb	5.7	1-Mar	6.4	19-Feb	7.1

Table 5. Average duration of the freezing season (days) during the historic period (1970–1999), the early (2000–2029), mid (2030–2059), and end-of-century (2060–2089) periods by emission scenario and site. The standard deviation is determined from 19 model CFI and CTI dates. NA values indicate that less than 80% of the models exceeded the CFI threshold.

	Stinson Lake (STI)				Madison (MAD)				Mariaville (MAR)				Kancamagus (KAN)				Lake Tarleton (LAK)			
Periods	RCP 4.5	SD (days)	RCP 8.5	SD (days)	RCP 4.5	SD (days)	RCP 8.5	SD (days)	RCP 4.5	SD (days)	RCP 8.5	SD (days)	RCP 4.5	SD (days)	RCP 8.5	SD (days)	RCP 4.5	SD (days)	RCP 8.5	SD (days)
Baseline (1970–1999)	93	2.1	93	2.1	79	1.9	79	1.9	64	2.9	64	2.9	85	2.6	85	2.6	80	2.7	80	2.7
Early century (2000–2029)	83	4.0	84	5.2	70	4.6	70	4.2	52	5.0	52	5.2	76	4.2	76	4.9	69	6.1	69	5.5
Mid-century (2030–2059)	73	6.8	66	9.2	59	7.0	56	7.7	NA	NA	NA	NA	66	6.7	59	8.3	57	6.8	53	5.0
End century (2060–2089)	65	9.1	48	6.8	54	6.2	NA	NA	NA	NA	NA	NA	59	7.3	NA	NA	49	8.2	NA	NA

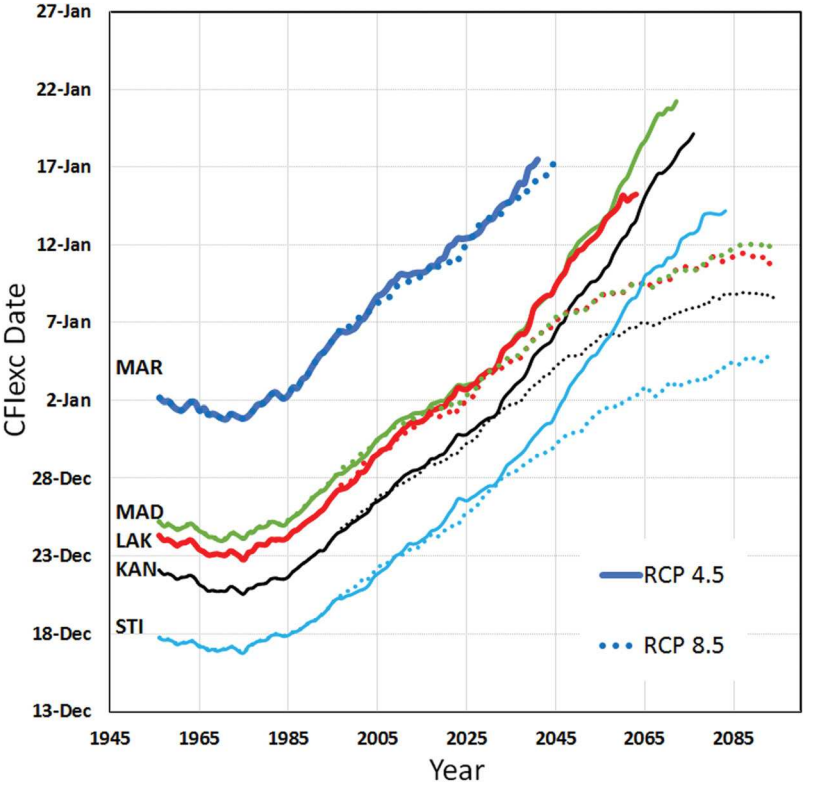

Figure 4. The projected CFI date for the five study sites. Each line represents the ensemble average of the 19 models using a 21-year moving average. The solid and stippled lines show the ensemble average for the higher and lower emission scenarios, respectively.

the calculations. Figure 8 shows projected future frost depths along with the calculated historical depths for the MAD, ME site. Frost depth will gradually decrease under both scenarios until approximately 2040, when the decrease in frost depth becomes more rapid under the high-emission scenario. Uncertainty in the models, as represented by the width of the 95% confidence interval, also increases over time.

Comparisons of frost depths by site are shown in Figure 9. Frost depth is a function of the climate/location, the number and thickness of the different pavement layers, and the materials in each pavement layer. Therefore, differences among sites are a function of those three variables. The KAN site has the deepest frost penetration of the five sites. The MAR site has the shallowest. All sites show that projected frost depths under the high-emission scenario become shallower at a greater rate than the low-emission scenario after approximately 2040. The rates of change vary from site to site, with sites that have deeper frost penetration generally showing larger changes over time and also larger differences between the low- and high-emission scenarios at the end of the century.

To isolate the effect of location and subgrade type, projected frost depths were calculated using two generic pavement cross-sections (Table 2). The only difference between the two cross-sections is the subgrade type. Figure 9(a) and (c) shows the results of this analysis for the MAD, MAR, and STI sites. As noted previously, because additional model calibrations were required for the LAK and KAN, application of a generic cross-section is not appropriate. Interestingly, for

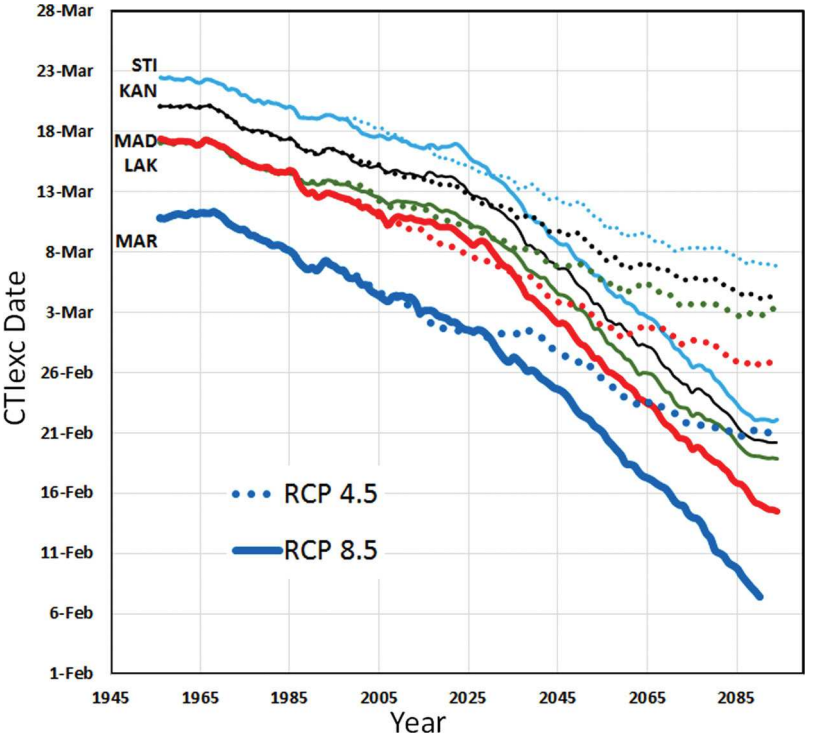

Figure 5. The projected CTI date for the five study sites. Each line represents the ensemble average of the 19 models using a 21-year moving average. The solid and stippled lines show the ensemble average for the higher and lower emission scenarios, respectively.

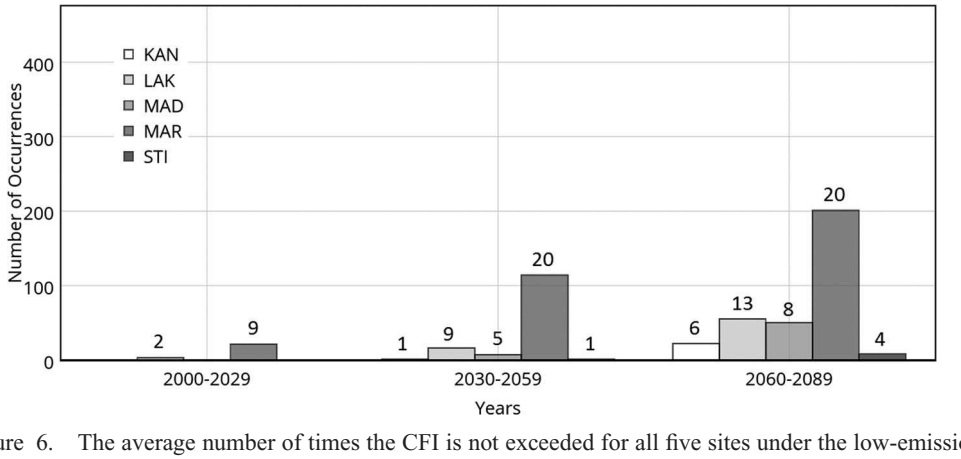

Figure 6. The average number of times the CFI is not exceeded for all five sites under the low-emission scenario. Each bar shows the average number of occurrences for all the models that project the CFI is not exceeded at each site during the respective time period. The number of models that comprise each average appears above each bar.

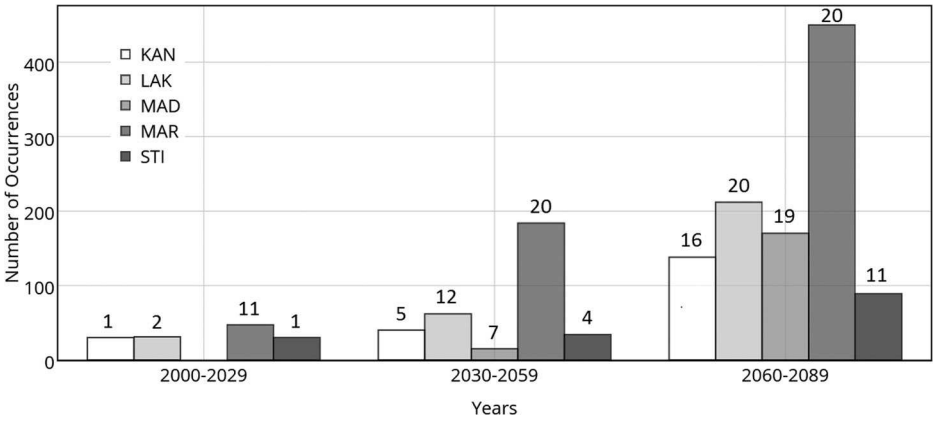

Figure 7. The average number of times the CFI is not exceeded for all five sites under the high-emission scenarios. Each bar shows the average number of occurrences for all the models that project the CFI is not exceeded at each site during the respective time period. The number of models that comprise each average appears above each bar.

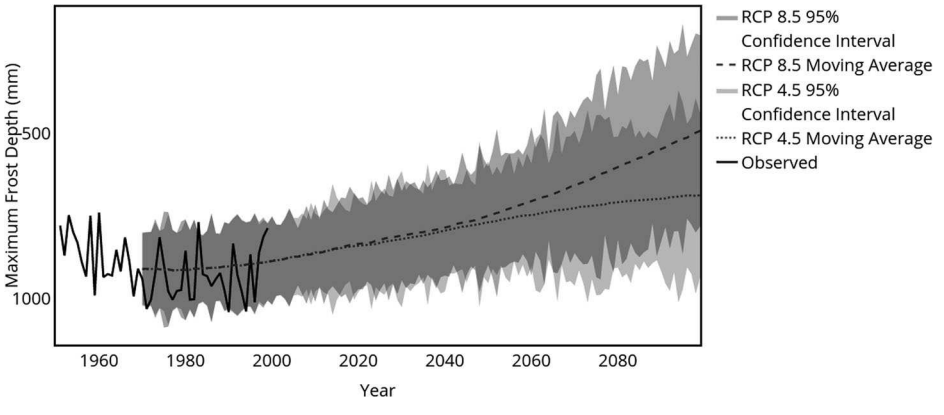

Figure 8. Observed and projected maximum frost depth for MAD, ME, based on RCP 4.5 and RCP 8.5 using a 21-year moving average. Shaded areas reflect the 95% confidence intervals of the climate models.

a specific subgrade type, differences in location caused a vertical offset for both generic cross-sections (Figure 9(a) and (c)). The clay subgrade (GEN1, Figure 9(a)) has a shallower frost depth overall and a smaller projected change over time (slope) and emission scenario as compared to the granular subgrade (GEN2, Figure 9(c)). The magnitude of difference due to location is smaller with the clay subgrade as well.

This finding indicates that the combination of the actual cross-sections and materials existing at a site with the site-specific climate can either amplify the effects of climate change or moderate the effects. Evaluation of the projected frost depths using the actual pavement cross-sections in combination with the two generic cross-sections shows that the actual MAD site has the shallowest slope and is very similar in magnitude and slope to the MAD GEN1 response. MAD is a silty clay subgrade, as is the GEN1 cross-section, so similar behaviour is expected. The actual MAR and STI are similar in terms of shape and magnitude of projected change, and fall between the responses from the GEN1 and GEN2 cross-sections. These two sites have silty sand, so it is reasonable that the response for these falls between the silty clay and granular responses. This analysis shows that both location and subgrade type influence the magnitude of the frost depths,

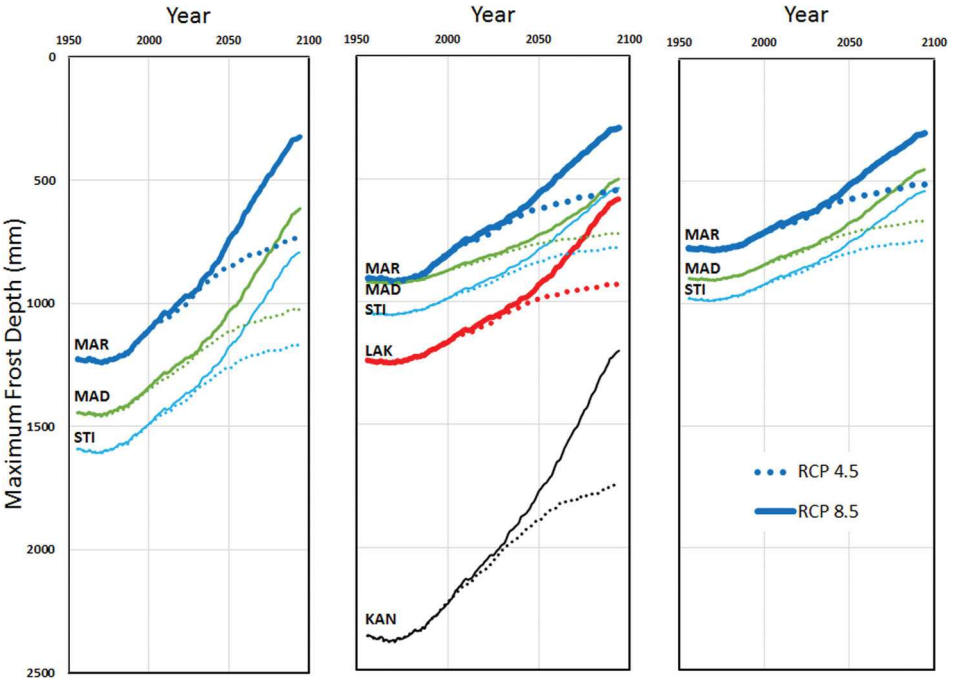

Figure 9. The projected maximum frost depths using (a) GEN1 pavement cross-section; (b) actual pavement cross-sections; and (c) GEN 2 pavement cross-section. Each line represents the ensemble average of the 19 models using a 21-year moving average. The solid and stippled lines show the ensemble average for the higher and lower emission scenarios, respectively.

whereas subgrade type is the primary factor influencing the rate at which projected changes will occur.

Summary and conclusions

This paper presents a study of future winter temperature changes and their potential impacts to freeze–thaw conditions in LVRs across Maine and New Hampshire study sites. Ensembles of 19 climate models with low- and high-emission scenarios were used to project future temperature changes. The impact of the temperature changes was determined for the maximum frost depth and the timing of WWPs and SLRs using established procedures for calculating cumulative frost and thaw indices. For both the freeze–thaw indices and the frost depths, variability was observed across the study region (approximately 150 km by 300 km), indicating that local conditions are important for future assessments depending upon the desired accuracy.

The study shows that the baseline (historic) timing for exceedance of the frost index threshold is mid-December to early January across the study region and reflects the influence of local climate. Modest shifts are expected early century; shifts of approximately 1 week are projected mid-century, while changes of 2 weeks are projected at the end of the century. For some locations, the high-emission scenario shows that the frost index will likely not be exceeded at the end of the century, indicating that the pavement will not completely freeze. Changes to spring thaw dates (as expressed by exceedance of the thaw index threshold) are projected to be of similar magnitudes. These results show that the duration for which the pavement cross-section is frozen will shorten by approximately 10 days every 30 years.

Shallower frost depths are projected for the end of the century. For a low-emission scenario, the maximum frost depth will be 250–500 mm shallower. For the high-emission scenario, the maximum frost depth will be up to 1000 mm shallower. The magnitude of the projected frost depth depends upon location and subgrade material type while the frost depth rate of change over the next 100 years is primarily influenced by material type, with granular materials showing larger rates of change than silty clay materials.

These projected changes in the freeze–thaw behaviour of LVRs may have significant effects on local communities, potentially leading to more rapid accumulation of damage or failure in these roads. These results indicate that the changes will be gradual which may make it difficult to detect given interannual differences. A priori knowledge of the likelihood of changes can make communities better able to mitigate impacts based on specific policies and practices. For example, the use of data-based assessments for determining the appropriate time to apply weight premiums and spring load restrictions will become more critical for preserving pavement condition under expected future climate conditions. The impacts of this on communities and policy development need further study.

Acknowledgements

The authors would like to acknowledge the contributions of Lee Friess, Ashley Fillion, and Tova Levin in this work.

Disclosure statement

No potential conflict of interest was reported by the authors.

Funding

This work was conducted through the Infrastructure and Climate Network (ICNet) project funded by the U.S. National Science Foundation research grant [CBET-1231326].

References

Andersland, O. B., & Ladanyi, B. (2004). *Frozen ground engineering*. Hoboken, NJ: John Wiley & Sons.

Barnett, T. P., Adams, J. C., & Lettenmeier, D. P. (2005). Potential impacts of a warming climate on water availability in snow-dominated regions. *Nature*, *438*, 303–309.

Berg, R., Kestler, M., Eaton, R., & Benda, C. (2006, July). *Estimating when to apply and remove spring load restrictions*. Paper presented at the Proceedings of the American Society of Civil Engineers 13th International Conference on Cold Regions Engineering, CD-ROM. Orono, ME.

Bianchini, A., & Gonzalez, C. R. (2012). *Pavement-Transportation Computer Assisted Structural Engineering (PCASE): Implementation of the modified Berggren (ModBerg) equation for computing the frost penetration depth within pavement structures* (Report # ERDC/GSL TR-12–15). Retrieved from http://www.dtic.mil/get-tr-doc/pdf?AD = ADA559915

Brekke, L., Thrasher, B., Maurer, E., & Pruitt, T. (2013). *Downscaled CMIP3 and CMIP5 climate and hydrology projections: Release of downscaled CMIP5 climate projections, comparison with preceding information, and summary of user needs*. Denver, CO: US Dept. of the Interior, Bureau of Reclamation, Technical Services Center.

Burakowski, E. A., Wake, C. P., Braswell, B., & Brown, D. P. (2008). Trends in wintertime climate in the northeastern United States: 1965–2005. *Journal of Geophysical Research: Atmospheres*, *113*, D20114. doi:10.1029/2008JD009870

Campbell, J. L., Ollinger, S. V., Flerchinger, G. N., Wicklein, H., Hayhoe, K., & Bailey, A. S. (2010). Past and projected future changes in snowpack and soil frost at the Hubbard Brook Experimental Forest, New Hampshire, USA. *Hydrological Processes*, *24*(17), 2465–2480.

Collins, M., Knutti, R., Arblaster, J., Dufresne, J.-L., Fichefet, T., Friedlingstein, P., … Krinner, G. (2013). Long-term climate change: Projections, commitments and irreversibility. In T. F. Stocker, D. Qin, G.-K. Plattner, M. Tignor, S. K. Allen, J. Boschung, … P. M. Midgley (Eds.), *Climate change 2013: The physical science basis. Contribution of working group I to the fifth assessment report of the intergovernmental panel on climate* (pp. 1029–1136). Cambridge: Cambridge University Press.

Cortez, E., Kestler, M., & Berg, D. (2000, February). *Computer-assisted calculations of the depth of frost penetration in pavement soils structures*. Paper presented at the Transportation Systems 2000 Workshop, San Antonio, TX.

Division, U. A. C. o. E. N. E. (1949). *Addendum No. 1 to report on frost investigation 1944–1945*. Boston, MA: Corps of Engineers, War Department.

Faiz, A. (2012). *The promise of rural roads: Review of the role of low-volume roads in rural connectivity, poverty reduction, crisis management, and livability* (Transportation Research E-Circular, E-C167). Retrieved from http://onlinepubs.trb.org/onlinepubs/circulars/ec167.pdf

Hayhoe, K., Wake, C. P., Huntington, T. G., Luo, L., Schwartz, M. D., Sheffield, J., … Wolfe, D. (2007). Past and future changes in climate and hydrological indicators in the US northeast. *Climate Dynamics*, *28*, 381–407. doi:10.1007/s00382-006-0187-8

Huntington, T. G., Hodgkins, G. A., Keim, B. D., & Dudley, R. W. (2004). Changes in the proportion of precipitation occurring as snow in New England (1949–2000). *Journal of Climate*, *17*, 2626–2636.

Kersten, M. S. (1949). *Laboratory research for the determination of the thermal properties of soils* (Technical Report 23). Hanover, NH: U.S. Army Cold Regions Research and Engineering Laboratory (CRREL).

Kestler, M., Berg, R., Miller, H., Steinert, B., Eaton, R., Larson, G., & Haddock, J. (2011). Keeping springtime low-volume road damage to a minimum: Toolkit of practical low-cost methods for road managers. *Transportation Research Record: Journal of the Transportation Research Board*, *2205*, 155–164.

Maurer, E., Wood, A., Adam, J., Lettenmaier, D., & Nijssen, B. (2002). A long-term hydrologically based dataset of land surface fluxes and states for the conterminous United States. *Journal of Climate*, *15*(22), 3237–3251.

Melillo, J. M., Richmond, T. T., & Yohe, G. (2014). *Climate change impacts in the United States*. Third National Climate Assessment. Retrieved from http://nca2014.globalchange.gov/downloads

Miller, H., Cabral, C., Kestler, M., Berg, R., & Eaton, R. (2013, June). *Comparative analyses of methods for posting spring load restrictions*. Paper presented at the Proceedings of the 10th International Symposium on Cold Regions Development, Anchorage, AK.

Miller, H. J., Cabral, C., Orr, D. P., Kestler, M. A., Berg, R., & Eaton, R. (2015). Modification of the US Army Corps of Engineers Model 158 for prediction of frost–thaw profiles in northern New England. *Transportation Research Record: Journal of the Transportation Research Board*, *2474*, 135–142.

Minnesota Department of Transportation. (2014). *Process for seasonal load limit starting and ending dates* (Technical Memorandum No. 14-10-MAT-02). Washington, DC: Transportation Research Board, National Research Council.

Orr, D. P., & Irwin, L. H. (2006). *Seasonal variations of in situ materials properties in New York state: Final report*. Ithaca, NY: Cornell Local Roads Program.

Stocker, T. F., Qin, D., Plattner, G. -K., Tignor, M., Allen, S. K., Boschung, J., … Midgley, P. M. (Eds.). (2013). *Summary for policymakers climate change 2013: The physical science basis. Contribution of working group I to the fifth assessment report of the intergovernmental panel on climate change*. Cambridge: Cambridge University Press.

TranSafety, I. (1997). *Road Management & Engineering Journal*. Retrieved from http://www.usroads.com/jounals/rej/re970204.htm

Van Deusen, D., Schrader, C., Bullock, D., & Worel, B. (1998). *Recent research on springtime thaw weakening and load restrictions* (Paper No. 98-0621; Transportation Research Record No. 1615). Washington D.C.: Transportation Research Board, National Research Council.

Wood, A. W., Maurer, E. P., Kumar, A., & Lettenmaier, D. P. (2002). Long-range experimental hydrologic forecasting for the eastern United States. *Journal of Geophysical Research: Atmospheres*, *107*, D20.